Stem Cell Reports
Report
ISSCR
OPEN ACCESS

Using Human Induced Pluripotent Stem Cell-Derived Cardiomyocytes as a Model to Study *Trypanosoma cruzi* Infection

Adriana Bozzi,[1,6] Nazish Sayed,[1,2,3] Elena Matsa,[1,2,3] Gabriele Sass,[4,5] Evgenios Neofytou,[1,2,3] Karl V. Clemons,[4,5] Rodrigo Correa-Oliveira,[6] David A. Stevens,[4,5] and Joseph C. Wu[1,2,3,*]

[1]Stanford Cardiovascular Institute, 265 Campus Drive, Rm G1120B, Stanford, CA 94305, USA
[2]Department of Medicine, Division of Cardiovascular Medicine, Stanford University, School of Medicine, Stanford, CA 94305, USA
[3]Department of Radiology, Stanford University, School of Medicine, Stanford, CA 94305, USA
[4]Division of Infectious Diseases and Geographic Medicine, Stanford University, School of Medicine, Stanford, CA 94305, USA
[5]California Institute for Medical Research, San Jose, CA 95128, USA
[6]Instituto René Rachou, FIOCRUZ, Belo Horizonte, Brazil
*Correspondence: joewu@stanford.edu
https://doi.org/10.1016/j.stemcr.2019.04.017

SUMMARY

Chagas disease (ChD) is one of the most neglected tropical diseases, with cardiomyopathy being the main cause of death in *Trypanosoma cruzi*-infected patients. As the parasite actively replicates in cardiomyocytes (CMs), the heart remains a key target organ in the pathogenesis of ChD. Here we modeled ChD using human induced pluripotent stem cell-derived CMs (iPSC-CMs) to understand the complex interplay between the parasite and host cells. We showed that iPSC-CMs can get infected with the *T. cruzi* Y strain and that all parasite cycle stages can be identified in our model system. Importantly, characterization of *T. cruzi*-infected iPSC-CMs showed significant changes in their gene expression profile, cell contractility, and distribution of key cardiac markers. Moreover, these infected iPSC-CMs exhibited a pro-inflammatory profile as indicated by significantly elevated cytokine levels and cell-trafficking regulators. We believe our iPSC-CM model is a valuable platform to explore new treatment strategies for ChD.

INTRODUCTION

Chagas disease (ChD) is a parasitic, systemic, and chronic disease caused by the protozoan *Trypanosoma cruzi*, with at least 6 million people estimated to be infected worldwide. *T. cruzi* parasites are mainly transmitted to humans by the infected feces of blood-sucking triatomine bugs often known as the "kissing bug". Despite intensive efforts to control this disease over the years, ChD has recently experienced a resurgence in endemic countries and emerged in non-endemic areas, such as the United States (due to factors such as immigration, blood transfusion, and organ transplantation) (Bern et al., 2011). Currently available therapeutic options for ChD are limited, with benznidazole (BNZ) or nifurtimox being recommended for treatment of acute phase and early in the chronic infection (de Andrade et al., 1996).

Characterized by a progressive inflammatory reaction, ChD presents an acute phase, generally asymptomatic, followed by a lifelong chronic phase, with distinct clinical forms known as indeterminate, cardiac (CARD), and digestive (Brener, 1980). The most common and severe manifestation of ChD is the CARD form that causes congestive heart failure, arrhythmias, and conduction abnormalities, often leading to stroke and sudden death. This type of dilated cardiomyopathy (DCM) is characterized by chronic inflammation, fibrosis, cardiac hypertrophy, and thromboembolic events. During its obligate intracellular stage, *T. cruzi* trypomastigotes can actively replicate in many different cell types such as macrophages, smooth and skeletal muscles, cardiomyocytes (CMs), and endothelial cells. Many studies investigating the immune response following *T. cruzi* infection and pathogenesis in the chronic phase of ChD have shown that the inflammatory response in the myocardium is an important aspect in the pathogenesis of ChD (Gomes et al., 2003; Sousa et al., 2014; Souza et al., 2004).

CARD is clearly the result of an inflammatory process. Therapeutic measures are aimed at treating the consequences of disease such as cardiac failure. This scenario necessitates attention to efficient diagnosis, treatment, and clinical management (Andrade et al., 2014). To this end, it is essential to improve our understanding of the progression of parasitic infection and standardization of models designed for ChD drug discovery. Rodents are the most commonly used models to study ChD, but fundamental differences between mice/rats and humans make murine models less than optimal for the following reasons: (1) the murine resting heart rate is approximately 6- to 10-fold faster than the human rate and (2) murine and human CMs also differ in fundamental aspects such as cardiac development, electrical properties, and ion channel contributions. As an alternative, in this study we developed a new model to study ChD using human induced pluripotent cell-derived CMs (iPSC-CMs).

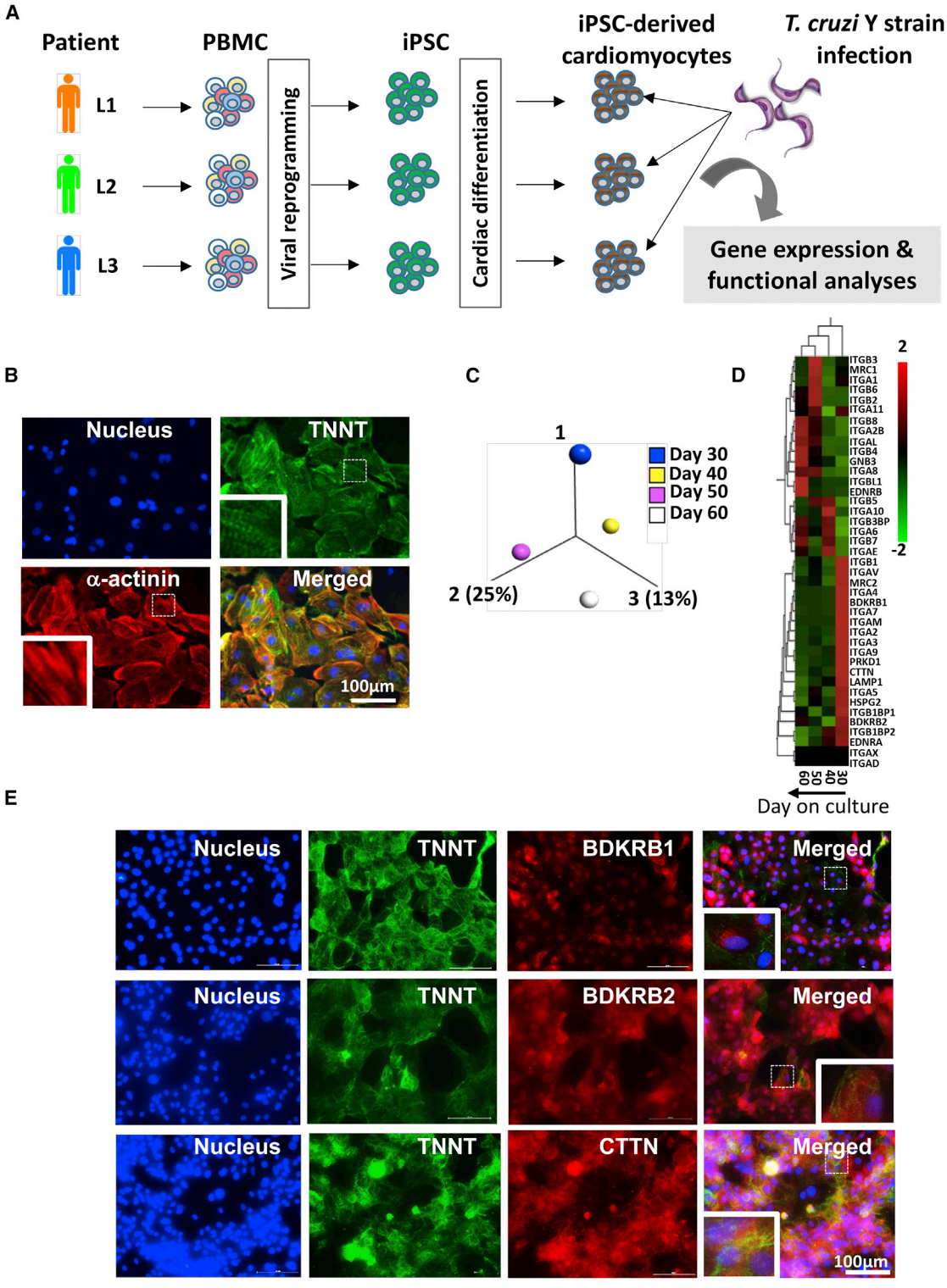

Figure 1. Human iPSC-CMs and Receptors to *Trypanosoma cruzi* Invasion

(A) Overview of study design. PBMCs from three healthy individuals were reprogrammed to iPSCs using a Sendai virus vector expressing Oct4, Sox2, Klf4, and c-Myc. iPSC clones were differentiated into iPSC-CMs, infected with *T. cruzi* Y strain, and submitted for gene expression and functional analysis.

(legend continued on next page)

RESULTS

Receptors to *T. cruzi* Invasion Are Expressed on iPSC-CMs

Peripheral blood mononuclear cells (PBMCs) from three healthy subjects were reprogrammed to iPSCs using the non-integrating Sendai virus method (Figure 1A). We achieved up to 90% efficiency in differentiating iPSC-CMs, as assessed by α-actin and troponin T expression and spontaneously contractility of iPSC-CMs (Figure 1B). Next, these iPSC-CMs were tested for their capacity to be infected by *T. cruzi* trypomastigotes. The gene expression of host receptors used by *T. cruzi* parasites to invade cells was analyzed in uninfected iPSC-CMs cultured on days 30, 40, 50, and 60. Principal-component analysis (PCA) (Figure 1C) and heatmap (Figure 1D) showed a differential gene expression pattern depending on the days being analyzed. The majority of receptors showed a high gene expression on day 30. We confirmed by immunofluorescence assay the expression of bradykinin receptor-1, bradykinin receptor-2, and cortactin in more than 80% of iPSC-CMs (Figure 1E), suggesting that parasitic infection of iPSC-CMs was possible starting on day 30.

Index of *T. cruzi* Infection in iPSC-CMs

The potential of *T. cruzi* (Tc) Y strain to invade iPSC-CMs was verified after 3 and 24 h interaction, in ratios of 1:5 and 1:10 (iPSC-CMs:parasites), respectively. The infection index grew with time interaction and ratio analyzed. A ratio of 1:10 enabled infection of 100% of iPSC-CMs by 24 h, therefore the higher ratio was not required (Figure 2A). Almost 50% of iPSC-CMs had the amastigote *T. cruzi* forms in their cytoplasm in a low ratio (1:5) after interaction (3 h). Therefore, all further infections were performed with 3 h interaction and at 1:5 ratio.

Time Course of *T. cruzi* Infection in iPSC-CMs

To explore *T. cruzi* infection in iPSC-CMs, we next analyzed the time course of infection. The number of amastigote form parasites increased exponentially and trypomastigote form parasites were observed in supernatant at 96 h of infection (Figure 2B). Importantly, the number of iPSC-CMs decreased significantly with around 91% rendered nonviable when infected with *T. cruzi* as compared with only 11% in the absence of infection (Figure 2C). Moreover, this decrease was further exacerbated following 72 and 96 h of infection (Figure 2D), and the morphology of the iPSC-CMs started to change to a vacuolated cytoplasm. At the same time-points, significant levels ($p < 0.05$) of reactive oxygen species (ROS) and reactive nitrogen species (RNS) were quantified in the supernatant of iPSC-CMs cultured with Tc Y strain (Figure 2E), suggesting that *T. cruzi* infection led to oxidative stress and apoptosis in iPSC-CMs.

iPSC-CM Contractility following *T. cruzi* Infection

All human iPSC-CM lines cultured with Tc Y strain were measured for their beat rate, peak height, and beat duration following 24 and 48 h of infection (Figures S1A–S1C). After 48 h of infection, iPSC-CMs were beating at nearly 200 beats per minute and experienced a significant increase in their peak height that was 3.27 times greater than that detected in the controls (Figures S1A and S1B). Although the differences in the beat duration were not significant, they were 11.83 times lower in non-infected iPSC-CMs (Figure S1C). These results were similar in all iPSC-CM lines. Next, we investigated the effects of *T. cruzi* infection on genes that encode calcium-handling proteins. We analyzed the gene expression level of *CACNA1C* (voltage-dependent L-type calcium channel), *RYR2* (ryanodine receptor 2), *CASQ2* (calsequestrin 2), *TRDN* (triadin), and *ATP2A2* (sarco(endo)plasmic reticulum calcium-ATPase 2 (Figure S2A). The majority of Ca^{2+} handling genes analyzed were downregulated in iPSC-CMs following *T. cruzi* infection. Moreover, we found low expression of *PKP2* gene (Figure S2B) that codes for the desmosomal protein plakophilin-2 and plays an important role in cell-cell adhesion and transcription of genes that control intracellular calcium cycling. Taken together, these data suggest that our iPSC-CM model reproduced an arrhythmic stress during *T. cruzi* infection that was characterized by tachycardia.

Sarcomeric Proteins and Connexin 43 Distribution in iPSC-CMs

To investigate the influence of *T. cruzi* infection on sarcomere structure and cell junction formation in iPSC-CMs, we tracked the distribution of α-actinin, troponin T, and connexin 43 during the course of infection (Figure S1D). While the non-infected iPSC-CMs had organized myofibrils with α-actinin and troponin T staining at the Z line of sarcomeres at all times-points (Figure S1D), the infected samples exhibited sarcomeric disarray as early as 24 h post-infection, which increased throughout the course of infection (48–96 h) (Figure S1D). The sarcomere localization of troponin T was similar to control cells

(B) Immunofluorescence images of iPSC-CMs confirming the presence of sarcomeric proteins such as α-actinin and troponin T.
(C and D) Variability in gene expression of receptors for *T. cruzi* invasion on iPSC-CMs cultured on days 30, 40, 50, and 60. (C) PCA with computation of closest neighboring samples; (D) heatmap showing hierarchical clustering between iPSC-CMs cultured on different days.
(E) Immunofluorescence images of iPSC-CMs showing the expression of receptors to *T. cruzi* such as bradykinin receptor 1 (BDKR1), bradykinin receptor 2 (BDKR2), and cortactin (CTTN). The expression of TNNT was used as a control. Scale bars, 100 μm.

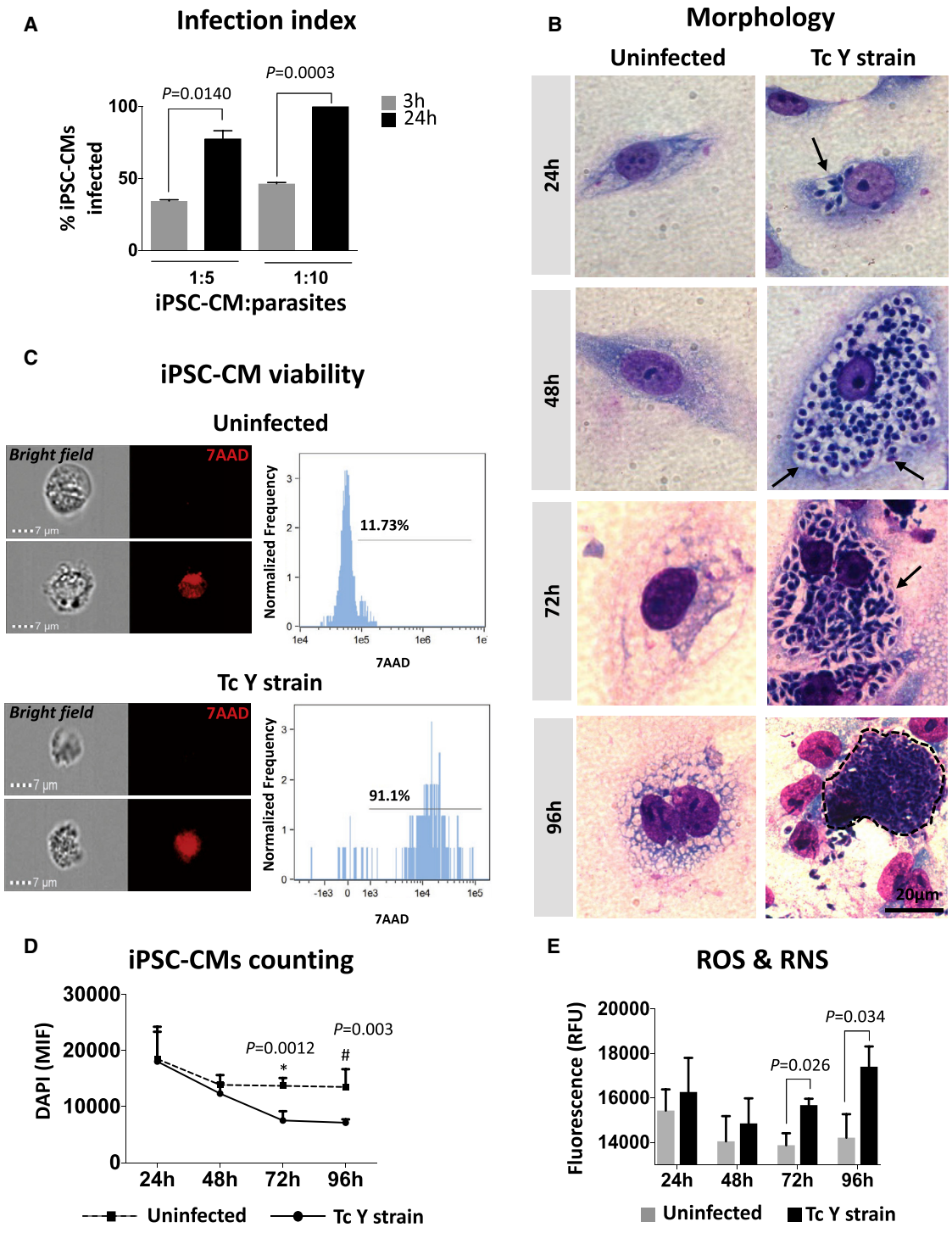

Figure 2. Infection of Human iPSC-CMs with *Trypanosoma cruzi*

(A) iPSC-CMs were cultured with *T. cruzi* (Tc) Y strain at the ratio 1:5 or 1:10 (iPSC-CMs:parasites) for 3 or 24 h. The percentage of iPSC-CMs with amastigote forms inside the cytoplasm was plotted as the average of three different counting areas. Significant statistical differences ($p < 0.05$) are indicated between samples.

(B) iPSC-CMs uninfected and infected with Tc Y strain in a ratio of 1:5 were stained with Giemsa after 24, 48, 72, and 96 h. The arrows point to amastigote *T. cruzi* forms in iPSC-CMs' cytoplasm, and the dotted line surrounds a nest of trypanomastigote *T. cruzi* outside ruptured iPSC-CMs. Scale bar, 20 µm.

(legend continued on next page)

until 48 h after *T. cruzi* infection. Following 72 and 96 h of infection, troponin T lost periodicity in the Z line of cardiac myofibrils (Figure S1D, Tc Y strain). By analyzing the connexin 43 distribution, we observed a loss of cell-cell junction at 24 h post-infection, which became more obvious at later timepoints (48–96 h) (Figure S1D, Tc Y strain).

Cytokines and Chemokines Secreted by iPSC-CMs following *T. cruzi* Infection

To investigate iPSC-CMs in relation to the inflammation in ChD, we next analyzed the secretion of cytokines and chemokines by iPSC-CMs following *T. cruzi* infection. Although CMs do not typically produce cytokines and chemokines, significant levels were found after 48 h of *T. cruzi* infection (Figure 3). Interestingly, these results showed a predominance of inflammatory activators (Figures 3A and 3B) compared with regulators (Figure 3C).

iPSC-CM Gene Expression Affected by *T. cruzi* Infection

We next performed RNA sequencing (RNA-seq) to analyze the iPSC-CM gene expression as described previously (Zhao et al., 2017). Uninfected and Tc Y strain-infected samples were grouped separately according to PCA analysis, which showed variability in gene expression before and after *T. cruzi* infection (Figure S3A). Heatmap analysis found approximately 11,000 genes that were differentially expressed ($p < 0.05$) following *T. cruzi* infection (Figure S3B). As ChD is characterized by an inflammatory process that results in progressive fibrosis affecting ventricular contractility and structure, we focused on the expression of genes that are related to cardiac remodeling, inflammation, and contractility. We found 78 genes that were significantly down- or up-regulated in iPSC-CMs infected with *T. cruzi*, and we compared these results with previously published gene expression analyses of other cardiomyopathies induced by Coxsackievirus (COX) (Sharma et al., 2014), familial DCM (Sun et al., 2012), and doxorubicin (DOX) (1 and 10 mM) (Burridge et al., 2016) (Figure 4A). All experiments were performed in a comparable manner including having similar differentiation protocols and seeding densities of iPSC-CMs. Similarly, close attention was paid to make sure that identical amounts of iPSC-CMs were seeded and exposed to *T. cruzi* when compared with uninfected controls. In contrast to COX, DCM, and DOX, iPSC-CMs infected with *T. cruzi* for 24 h showed inflammatory activity with a high expression of genes for chemoattractant and adhesion proteins (*CXCL3*, *CXCL6*, *CXCL12*, *CXCL14*, *CXCL17*, and *CLEC4D*) and pro-inflammatory proteins (*IL6ST*, *IL-9R*, *TNFAIP1*, *IRAK1*, *MRC2*, and *HMGB1*) (Figure 4B). Furthermore, genes expressing extracellular matrix proteins such as collagen type I and IV (*COL1A1*, *COL1A2*, and *COL4A4*), laminin (*LAMA1*), and metalloproteinase (*MMP9* and *MMP24*) were significantly expressed in iPSC-CMs infected with *T. cruzi*. Interestingly, the majority of genes for sarcomeric proteins (*ACTA2*, *MYH11*, *MYL2*, *MYBPC3*, *TNNC1*, *TNNT2*, and *TMOD1*) and cytoskeleton (*DMD* and *VCL*) were downregulated in our iPSC-CM model following *T cruzi* infection (Figure 4C), which correlated well with the vacuolated morphology of infected iPSC-CMs.

DISCUSSION

This study was designed to develop an *in vitro* platform using human cardiac cells to study ChD that remains a public health problem in affected regions. As ~30%–40% of all Chagasic patients exhibit a severe clinical phenotype including heart failure, there is a compelling need to understand the mechanisms involved in ChD using human cardiac cells. Even though ChD has been studied previously using human PBMCs (Gomes et al., 2014; Sousa et al., 2014) or murine models (Garzoni et al., 2003; Pereira et al., 1993), it has been difficult to model ChD in human cardiac cells due to lack of available human samples. Our group has successfully reprogrammed adult cells into iPSCs (Churko et al., 2013) and differentiated them into CMs (Burridge et al., 2014), thereby providing an ideal *in vitro* platform for modeling human cardiac diseases (Liu et al., 2018; Sayed et al., 2016; Sharma et al., 2017), drug screening (Liang et al., 2013; Matsa et al., 2016), and precision medicine (Sayed et al., 2019; Sayed and Wu, 2017). Until now, this platform has not been used to model cardiac diseases that are triggered by parasitic infection such as *T. cruzi*. Here, we generated an iPSC-CM model that can be infected by Tc Y strain to recapitulate all phases of the parasite's life cycle including: (1) infective stage, (2) trypomastigotes

(C) iPSC-CM viability assay: images (bright and 7-AAD fluorescence fields) and histograms representatives of iPSC-CMs uninfected and infected with Tc Y strain stained with 7-AAD.

(D) Number of iPSC-CMs over the time course of *T. cruzi* infection. iPSC-CMs uninfected (dotted line) and infected (Tc Y strain) were stained with DAPI and the nucleus counted by size. The graph shows the average of triplicates of the iPSC-CMs after exclusion of trypanomastigote nuclei. Significant statistical differences ($p < 0.05$) are indicated among samples.

(E) Total production of free radicals. Reactive oxygen species and reactive nitrogen species (ROS/RNS) were measured in the supernatants of iPSC-CMs uninfected and infected with Tc Y strain (1:5, 3 h interaction). The average of biological triplicates is expressed in columns graphs. Significant statistical differences are indicated among samples ($p < 0.05$).

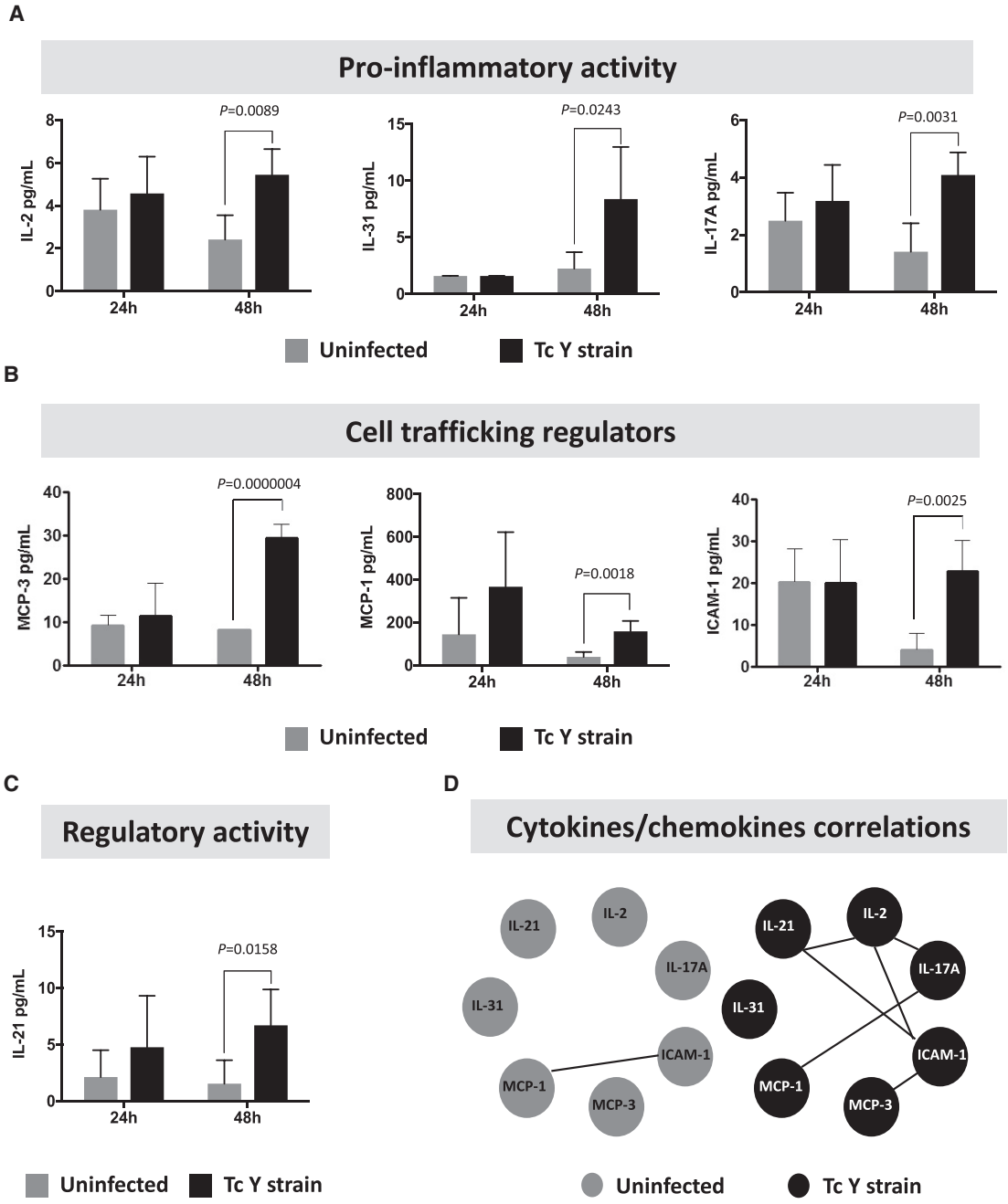

Figure 3. Regulators of Inflammation Delivered by iPSC-CMs Infected with *T. cruzi*

(A–C) Sixty-three human molecules were measured in the supernatants of iPSC-CMs uninfected and infected with *T. cruzi* (Tc Y strain) (1:5, 3 h interaction). Graphs shows most significantly affected (A) pro-inflammatory cytokines, (B) cell trafficking regulators, and (C) regulatory cytokines produced by iPSC-CMs following 24 and 48 h *T. cruzi* infection. Significant statistical differences are indicated among samples ($p < 0.05$).

(D) Significant positive correlation between cytokines and chemokines produced by iPSC-CMs at 48 h *T. cruzi* infection ($p < 0.05$; Spearman and Pearson correlation). These results are averages of three different iPSC-CM lines, with each line being tested in duplicates.

transforming into amastigotes, (3) multiplying amastigotes, (4) amastigotes transforming into trypomastigotes, and (5) trypomastigotes bursting out of host cells.

ChD has an acute and a chronic phase, in which the acute phase is the first contact between the parasite and the host that is usually asymptomatic and characterized

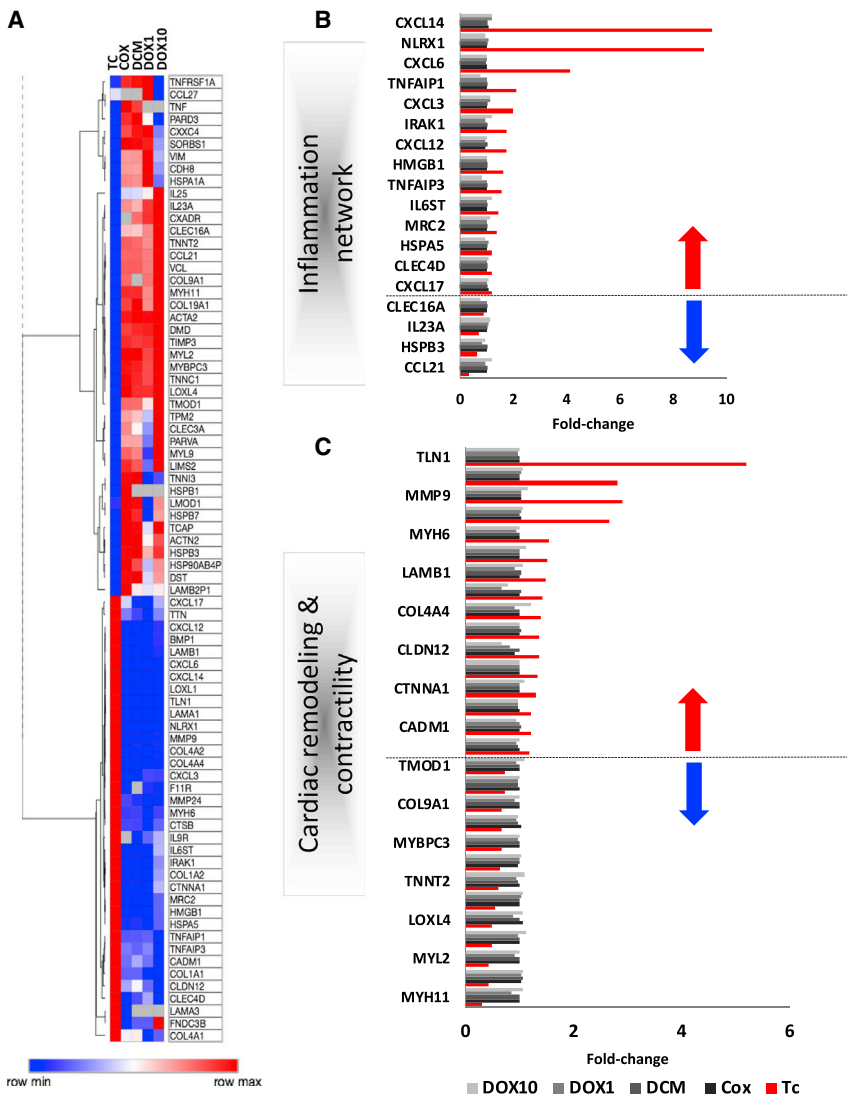

Figure 4. Comparing Gene Expression Among Different Cardiomyopathies

(A) Significant genes expressed in iPSC-CMs infected with *T. cruzi* (Tc) (1:5, 3 h interaction) for 24 h were compared with gene expression of iPSC-CMs infected with Coxsackievirus (COX), iPSC-CMs from dilated cardiomyopathy (DCM) patients, or iPSC-CMs treated with doxorubicin 1 μM (DOX1) and 10 μM (DOX10).

(B and C) Differentially expressed genes in iPSC-CMs infected with *T. cruzi* compared with COX, DCM, DOX1, and DOX10. Graphs show genes related to the network of (B) inflammation, (C) cardiac remodeling and contractility. Red arrows indicate upregulated genes and blue arrows indicate downregulated genes.

by elevated parasitic load. In contrast, the chronic phase is characterized by subpatent parasitemia and disease progression (Menezes et al., 2011). In our study, we infected iPSC-CMs with *T. cruzi* that reflected both the acute phase (24 and 48 h) as well as the chronic phase (72 and 96 h), in which an exponential high parasitic load was observed (Figure 2B). This successful demonstration of human iPSC-CM infection with *T. cruzi* makes our model a valid *in vitro* platform to study disease mechanisms of ChD as well as understand host-parasite cell interactions. Furthermore, it provides a unique platform for screening new drugs in the management of ChD. To that end, our data showed that BNZ, the first line of drug for ChD, significantly reduced the percentage of iPSC-CMs infected with *T. cruzi* (Figure S4).

Clinically, ROS/RNS are elevated during the acute phase of *T. cruzi* infection; however, we detected ROS/RNS in iPSC-CMs during the chronic phase of our iPSC-CM model. This could be due to the different strains of *T. cruzi*, as ROS/RNS production depends on the pathogen's virulence (Andrade et al., 1999). We used the Y strain of *T. cruzi*, which is known to be less infective to myoblasts when compared with other strains, and thereby responsible for a low level of parasitemia (Andrade et al., 2010). In addition, *T. cruzi* has a very efficient antioxidant machinery that can regulate the immediate ROS production thereby allowing the parasite to evade the early host response.

Interestingly, the time course of *T. cruzi* infection mirrored some aspects of clinical manifestations observed in patients with ChD (Medeiros et al., 2017). The

co-existence of inflammatory infiltration and fibrosis in ChD results in an abnormal electrocardiogram characterized by arrhythmias, conduction disturbances, and repolarization changes (Spencer et al., 2011). Our iPSC-CMs showed a high beat rate, high peak height, and low beat duration matching arrhythmias in patients with ChD (Figures S1A–S1C). This resulting tachycardia may be due to altered distributions of sarcomeric proteins, α-actinin (contractility protein), troponin T (regulatory protein), and connexin 43 (gap junction protein), which happened at 72 h post-infection (Figure S1D). Moreover, it could also be due to the low expression of calcium-handling genes such as *RYR2*, *ANK2*, *CACNA1C*, *TRDN*, and *CASQ2* (Figure S2). Indeed, decreased CASQ2 levels have been linked to arrhythmias triggered by β-adrenergic stimulation (Tavi et al., 2005). Similarly, disruptions in α-actinin distribution in mouse embryonic CMs has been observed following 72 h of *T. cruzi* infection (Melo et al., 2006). Notably, in our model the *T. cruzi* infection interfered with sarcomere organization and intercellular junctions, which could explain the conduction disturbances seen in both acute and chronic patients with ChD.

Previous studies in ChD have analyzed gene expression in murine heart models (Henao-Martinez and Parra-Henao, 2015), but little is known about the variability in genome responses over the time course of the *T. cruzi* infection. Given that ChD is characterized by intense inflammatory infiltrates (Rocha et al., 2007), we analyzed the genes that can affect inflammation, cardiac remodeling, and contractility to assess the variations in gene expression signatures in ChD-infected iPSC-CMs. ChD is known to show a robust immune response orchestrated by innate immune cells with high levels of interleukin-12 (IL-12), interferon gamma, and tumor necrosis factor alpha (Andrade et al., 2014). Indeed, our infected iPSC-CMs showed a similar response with an increase in IL-2, IL-17A, MCP-1, and ICAM-1. However, the normal heart does not constitutively express inflammatory cytokines, suggesting that physical and/or chemical stresses due to *T. cruzi* infection might be responsible for the immune response from the CMs. This is consistent with findings in existing literature analyzing cytokine levels in PBMCs of patients with ChD (Gomes et al., 2014; Guedes et al., 2012). Furthermore, the increase in pro-inflammatory markers in iPSC-CMs correlated with the advent of iPSC-CM dysfunction, suggesting that these cytokine levels were high enough to trigger CM dysfunction. Finally, the comparison of gene expression between *T. cruzi* and other cardiomyopathies (Figure 4) revealed genes that could be used as potential targets to manage ChD, including *CXCL6*, *CXCL12*, *CXCL14*, and *CXCL17*, as these chemokines are known to contribute to the regulation of immune cell migration (Lu et al., 2016).

In summary, our study generates the first compelling data to demonstrate the feasibility of using human iPSCs to model ChD. We showed that human iPSC-CMs can be infected by the *T. cruzi* strain and can recapitulate the key aspects of cardiac dysfunction observed during ChD cardiomyopathy. Importantly, our study highlights a list of relevant genes that might play an important role in ChD pathogenesis, making them potential targets for pharmacological intervention. However, questions concerning the specificity of the drug effects still remain to be answered. We believe our study may pave the way to using the iPSC technology as an ideal platform to screen for novel anti-parasitic drugs against ChD cardiomyopathy.

EXPERIMENTAL PROCEDURES

An expanded section is available in the Supplemental Experimental Procedures. Human iPSCs were derived from fibroblasts or PBMCs obtained from patients using approved IRB protocols 17576 and 29904.

Differentiation of iPSC-CMs

iPSCs were differentiated into iPSC-CMs on Matrigel-coated plates using our established CM differentiation protocol (Burridge et al., 2014). In brief, iPSCs were treated with CHIR99021, a *Wnt* activator for 2 days followed by IWR treatment in RPMI medium plus B27 supplement without insulin. From day 7 onward, cells were placed in RPMI plus B27 medium until beating was observed. At this point, cells were glucose starved for 3–4 days to purify iPSC-CMs and further maintained RPMI plus B27 medium.

Invasion Assay with *T. cruzi*

Beating iPSC-CMs were plated in 24-well plates at 2×10^5 cells/well in RPMI plus B27 with insulin for the *T. cruzi* infection. To optimize the infection, we analyzed two target effector ratios, 1:5 and 1:10 (iPSC-CMs:parasites) at two time points (3 and 24 h) in a volume of 500 μL per well. An infection time-response curve was used to define the optimal time of infection for use in further analysis with biological assays. An uninfected group was subjected to the same conditions and medium, except for the presence of the parasite. This group represented the vehicle/mock group, and all the data from the *T. cruzi* infection group were compared with the uninfected group.

Statistical Analysis

PCA and hierarchical clustering heatmap analysis were performed for gene expression with Omics Explorer version 3.2 software (Qlucore, NY, USA). MANOVA test with $p < 0.05$ significance was used for comparisons. Statistical analyses for functional data were performed using Graph Pad Prism v7.0 software. Data are presented as mean ± SEM. Comparisons were conducted by Student's t test, using the Bonferroni-Dunn method or one-way ANOVA. Correlation analyses were done using Pearson or Spearman's correlation coefficient. Results were considered significant when $p < 0.05$.

ACCESSION NUMBERS

The GEO accession number for RNA-seq in this paper is GEO: GSE129676.

SUPPLEMENTAL INFORMATION

Supplemental Information can be found online at https://doi.org/10.1016/j.stemcr.2019.04.017.

AUTHOR CONTRIBUTIONS

A.B., conception and design, data collection, data analysis, and manuscript writing; N.S., conception and design, data analysis, and manuscript writing; E.M., data collection and data analysis; G.S., data collection and data analysis; E.N., data analysis; K.V.C., conception and design; R.C.O., conception, design, financial support, and manuscript writing; D.A.S., conception, design, financial support, and manuscript writing; J.C.W., conception and design, financial support, manuscript writing, and final approval of manuscript.

ACKNOWLEDGMENTS

We thank Ning-Yi Shao for RNA-seq analysis, Andréa Teixeira de Carvalho and Vitor Hugo Simões Miranda for viability assay analysis, and Juliana de Assis Silva Gomes Estanislau for critical reading of the manuscript. We gratefully acknowledge funding support from the NIH (R01 HL133272, R01 HL130020, R01 HL128170, and R01 HL132875), Burroughs Wellcome Fund IRSA 1015009 (J.C.W.), NIH K01 HL135455, Stanford TRAM scholar grant (N.S.), Conselho Nacional de Desenvolvimento Científico e Tecnológico (R.C.O.), Stanford CVI seed grant (A.B.), and the California Institute for Medical Research (D.A.S.). J.C.W. is a co-founder of Khloris Biosciences but has no competing interests, as the work presented was performed independently.

Received: February 2, 2018
Revised: April 18, 2019
Accepted: April 19, 2019
Published: May 16, 2019

REFERENCES

Andrade, D.V., Gollob, K.J., and Dutra, W.O. (2014). Acute Chagas disease: new global challenges for an old neglected disease. PLoS Negl. Trop. Dis. *8*, e3010.

Andrade, L.O., Galvao, L.M., Meirelles Mde, N., Chiari, E., Pena, S.D., and Macedo, A.M. (2010). Differential tissue tropism of *Trypanosoma cruzi* strains: an in vitro study. Mem. Inst. Oswaldo Cruz. *105*, 834–837.

Andrade, L.O., Machado, C.R., Chiari, E., Pena, S.D., and Macedo, A.M. (1999). Differential tissue distribution of diverse clones of *Trypanosoma cruzi* in infected mice. Mol. Biochem. Parasitol. *100*, 163–172.

Bern, C., Kjos, S., Yabsley, M.J., and Montgomery, S.P. (2011). *Trypanosoma cruzi* and Chagas' disease in the United States. Clin. Microbiol. Rev. *24*, 655–681.

Brener, Z. (1980). Immunity to *Trypanosoma cruzi*. Adv. Parasitol. *18*, 247–292.

Burridge, P.W., Li, Y.F., Matsa, E., Wu, H., Ong, S.G., Sharma, A., Holmström, A., Chang, A.C., Coronado, M.J., Ebert, A.D., et al. (2016). Human induced pluripotent stem cell-derived cardiomyocytes recapitulate the predilection of breast cancer patients to doxorubicin-induced cardiotoxicity. Nat. Med. *22*, 547–556.

Burridge, P.W., Matsa, E., Shukla, P., Lin, Z.C., Churko, J.M., Ebert, A.D., Lan, F., Diecke, S., Huber, B., Mordwinkin, N.M., et al. (2014). Chemically defined generation of human cardiomyocytes. Nat. Methods *11*, 855–860.

Churko, J.M., Burridge, P.W., and Wu, J.C. (2013). Generation of human iPSCs from human peripheral blood mononuclear cells using non-integrative Sendai virus in chemically defined conditions. Methods Mol. Biol. *1036*, 81–88.

de Andrade, A.L., Zicker, F., de Oliveira, R.M., Almeida Silva, S., Luquetti, A., Travassos, L.R., Almeida, I.C., de Andrade, S.S., de Andrade, J.G., and Martelli, C.M. (1996). Randomised trial of efficacy of benznidazole in treatment of early *Trypanosoma cruzi* infection. Lancet *348*, 1407–1413.

Garzoni, L.R., Masuda, M.O., Capella, M.M., Lopes, A.G., and de Meirelles Mde, N. (2003). Characterization of $[Ca^{2+}]_i$ responses in primary cultures of mouse cardiomyocytes induced by *Trypanosoma cruzi* trypomastigotes. Mem. Inst. Oswaldo Cruz. *98*, 487–493.

Gomes, J.A., Bahia-Oliveira, L.M., Rocha, M.O., Martins-Filho, O.A., Gazzinelli, G., and Correa-Oliveira, R. (2003). Evidence that development of severe cardiomyopathy in human Chagas' disease is due to a Th1-specific immune response. Infect. Immun. *71*, 1185–1193.

Gomes, J.A., Molica, A.M., Keesen, T.S., Morato, M.J., de Araujo, F.F., Fares, R.C., Fiuza, J.A., Chaves, A.T., Pinheiro, V., Nunes Mdo, C., et al. (2014). Inflammatory mediators from monocytes down-regulate cellular proliferation and enhance cytokines production in patients with polar clinical forms of Chagas disease. Hum. Immunol. *75*, 20–28.

Guedes, P.M., Gutierrez, F.R., Silva, G.K., Dellalibera-Joviliano, R., Rodrigues, G.J., Bendhack, L.M., Rassi, A., Jr., Rassi, A., Schmidt, A., Maciel, B.C., et al. (2012). Deficient regulatory T cell activity and low frequency of IL-17-producing T cells correlate with the extent of cardiomyopathy in human Chagas' disease. PLoS Negl. Trop. Dis. *6*, e1630.

Henao-Martinez, A.F., and Parra-Henao, G. (2015). Murine heart gene expression during acute Chagasic myocarditis. Genomics Data *4*, 76–77.

Liang, P., Lan, F., Lee, A.S., Gong, T., Sanchez-Freire, V., Wang, Y., Diecke, S., Sallam, K., Knowles, J.W., Wang, P.J., et al. (2013). Drug screening using a library of human induced pluripotent stem cell-derived cardiomyocytes reveals disease-specific patterns of cardiotoxicity. Circulation *127*, 1677–1691.

Liu, C., Oikonomopoulos, A., Sayed, N., and Wu, J.C. (2018). Modeling human diseases with induced pluripotent stem cells: from 2D to 3D and beyond. Development *145*. https://doi.org/10.1242/dev.156166.

Lu, J., Chatterjee, M., Schmid, H., Beck, S., and Gawaz, M. (2016). CXCL14 as an emerging immune and inflammatory modulator. J. Inflamm. (Lond.) *13*, 1.

Matsa, E., Burridge, P.W., Yu, K.H., Ahrens, J.H., Termglinchan, V., Wu, H., Liu, C., Shukla, P., Sayed, N., Churko, J.M., et al. (2016). Transcriptome profiling of patient-specific human iPC-cardiomyocytes predicts individual drug safety and efficacy responses in vitro. Cell Stem Cell *19*, 311–325.

Medeiros, N.I., Fares, R.C., Franco, E.P., Sousa, G.R., Mattos, R.T., Chaves, A.T., Nunes, M.D., Dutra, W.O., Correa-Oliveira, R., Rocha, M.O., and Gomes, J.A. (2017). Differential expression of matrix metalloproteinases 2, 9 and cytokines by neutrophils and monocytes in the clinical forms of Chagas disease. PLoS Negl. Trop. Dis. *11*, e0005284.

Melo, T.G., Almeida, D.S., Meirelles, M.N., and Pereira, M.C. (2006). Disarray of sarcomeric alpha-actinin in cardiomyocytes infected by *Trypanosoma cruzi*. Parasitology *133*, 171–178.

Menezes, C., Costa, G.C., Gollob, K.J., and Dutra, W.O. (2011). Clinical aspects of Chagas disease and implications for novel therapies. Drug Dev. Res. *72*, 471–479.

Pereira, M.C., Costa, M., Chagas Filho, C., and de Meirelles, M.N. (1993). Myofibrillar breakdown and cytoskeletal alterations in heart muscle cells during invasion by *Trypanosoma cruzi*: immunological and ultrastructural study. J. Submicrosc. Cytol. Pathol. *25*, 559–569.

Rocha, M.O., Teixeira, M.M., and Ribeiro, A.L. (2007). An update on the management of Chagas cardiomyopathy. Expert Rev. Anti. Infect. Ther. *5*, 727–743.

Sayed, N., Ameen, M., and Wu, J.C. (2019). Personalized medicine in cardio-oncology: the role of induced pluripotent stem cell. Cardiovasc. Res. *115*, 949–959.

Sayed, N., Liu, C., and Wu, J.C. (2016). Translation of human-induced pluripotent stem cells: from clinical trial in a dish to precision medicine. J. Am. Coll. Cardiol. *67*, 2161–2176.

Sayed, N., and Wu, J.C. (2017). Towards cardio-precision medicine. Eur. Heart J. *38*, 1014–1016.

Sharma, A., Burridge, P.W., McKeithan, W.L., Serrano, R., Shukla, P., Sayed, N., Churko, J.M., Kitani, T., Wu, H., Holmström, A., et al. (2017). High-throughput screening of tyrosine kinase inhibitor cardiotoxicity with human induced pluripotent stem cells. Sci. Transl. Med. *9*. https://doi.org/10.1126/scitranslmed.aaf2584.

Sharma, A., Marceau, C., Hamaguchi, R., Burridge, P.W., Rajarajan, K., Churko, J.M., Wu, H., Sallam, K.I., Matsa, E., Sturzu, A.C., et al. (2014). Human induced pluripotent stem cell-derived cardiomyocytes as an in vitro model for Coxsackievirus B3-induced myocarditis and antiviral drug screening platform. Circ. Res. *115*, 556–566.

Sousa, G.R., Gomes, J.A., Fares, R.C., Damásio, M.P., Chaves, A.T., Ferreira, K.S., Nunes, M.C., Medeiros, N.I., Valente, V.A., Corrêa-Oliveira, R., et al. (2014). Plasma cytokine expression is associated with cardiac morbidity in Chagas disease. PLoS One *9*, e87082.

Souza, P.E., Rocha, M.O., Rocha-Vieira, E., Menezes, C.A., Chaves, A.C., Gollob, K.J., and Dutra, W.O. (2004). Monocytes from patients with indeterminate and cardiac forms of Chagas' disease display distinct phenotypic and functional characteristics associated with morbidity. Infect. Immun. *72*, 5283–5291.

Spencer, N.D., Gimble, J.M., and Lopez, M.J. (2011). Mesenchymal stromal cells: past, present, and future. Vet. Surg. *40*, 129–139.

Sun, N., Yazawa, M., Liu, J., Han, L., Sanchez-Freire, V., Abilez, O.J., Navarrete, E.G., Hu, S., Wang, L., Lee, A., et al. (2012). Patient-specific induced pluripotent stem cells as a model for familial dilated cardiomyopathy. Sci. Transl. Med. *4*, 130ra147.

Tavi, P., Hansson, A., Zhang, S.J., Larsson, N.G., and Westerblad, H. (2005). Abnormal Ca(2+) release and catecholamine-induced arrhythmias in mitochondrial cardiomyopathy. Hum. Mol. Genet. *14*, 1069–1076.

Zhao, M.-T., Chen, H., Liu, Q., Shao, N.Y., Sayed, N., Wo, H.T., Zhang, J.Z., Ong, S.G., Liu, C., Kim, Y., et al. (2017). Molecular and functional resemblance of differentiated cells derived from isogenic human iPSCs and SCNT-derived ESCs. Proc. Natl. Acad. Sci. U S A *114*, E11111–E11120.

Stem Cell Reports, Volume *12*

Supplemental Information

Using Human Induced Pluripotent Stem Cell-Derived Cardiomyocytes as a Model to Study *Trypanosoma cruzi* Infection

Adriana Bozzi, Nazish Sayed, Elena Matsa, Gabriele Sass, Evgenios Neofytou, Karl V. Clemons, Rodrigo Correa-Oliveira, David A. Stevens, and Joseph C. Wu

Supplemental Figures and Legends

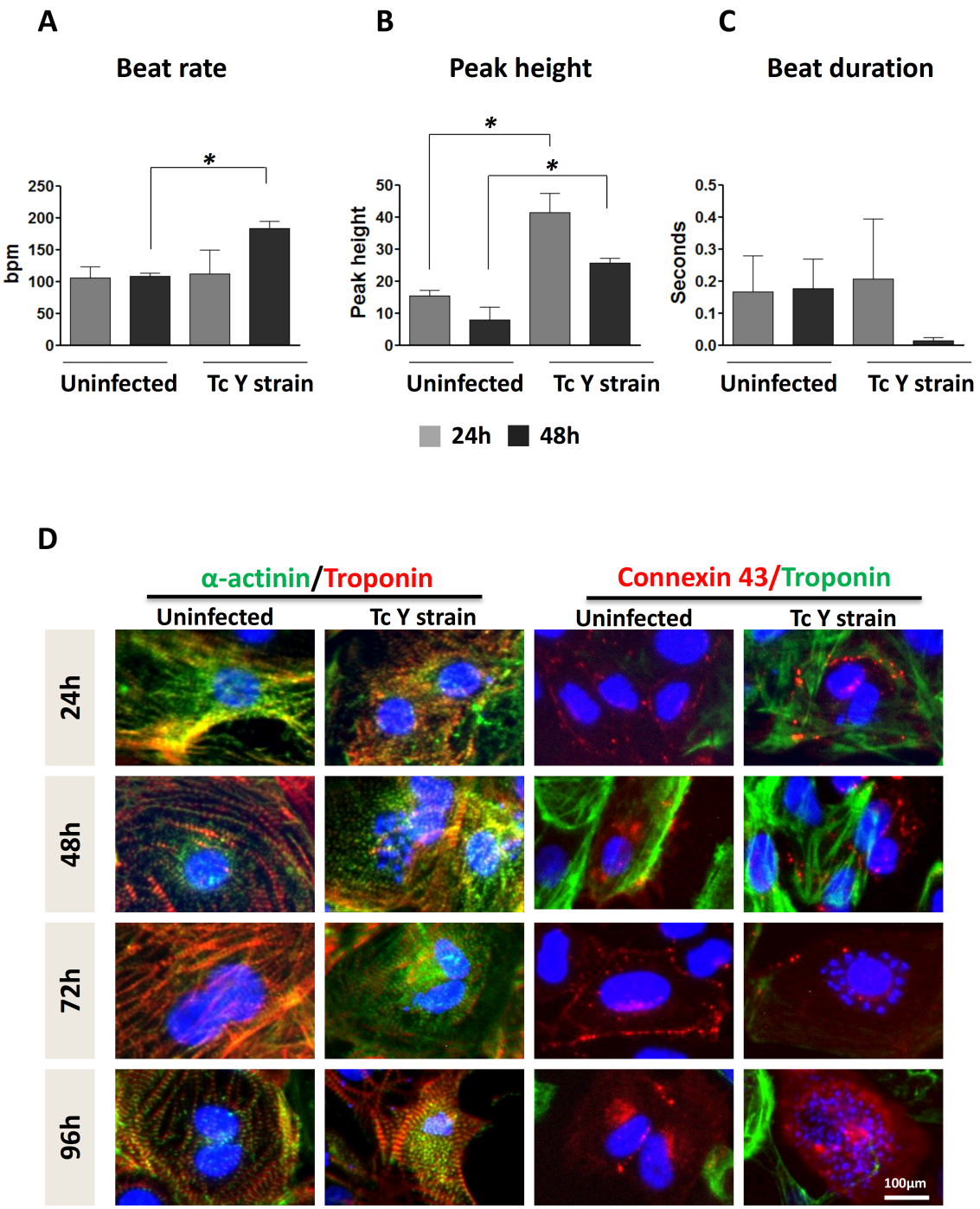

Figure S1. Related to Figure 2. Contractility and Sarcomeric Structure of iPSC-CMs after *T. cruzi* Infection. (A-C) Beat rate, peak height, and beat duration before and after *T. cruzi* infection at 24 and 48 hr. The average of biological triplicates is expressed in columns graphs. Significant statistical ($p<0.05$) differences are indicated between samples (*). **(D)** Immunofluorescence of iPSC-CMs uninfected and infected with Tc Y strain (1:5, 3 hr interaction) shows the distributions of α-actinin, troponin T, and Connexin 43 over the course of infection (24, 48, 72, and 96 hr).

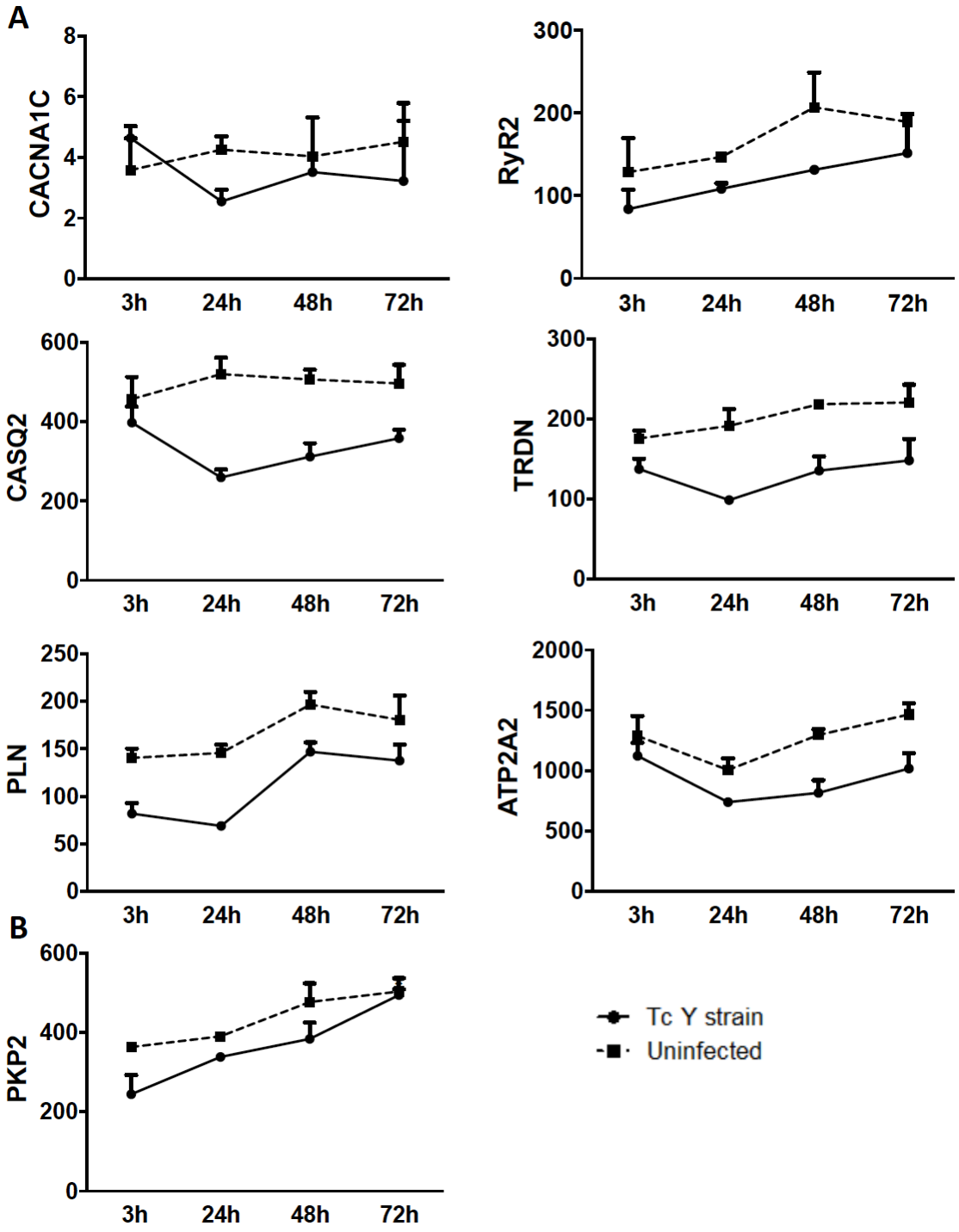

Figure S2. Related to Figure 4. Intracellular Calcium Cycling after *T. cruzi* Infection. (A) Gene expression for calcium handling genes *CACNA1C*, *RYR2*, *CASQ2*, *TRDN*, and *ATP2A*, and **(B)** for the desmosomal gene *PKP2* was analyzed in uninfected and infected (Tc Y strain) iPSC-CMs at different times. The average of biological duplicates is expressed in graphs.

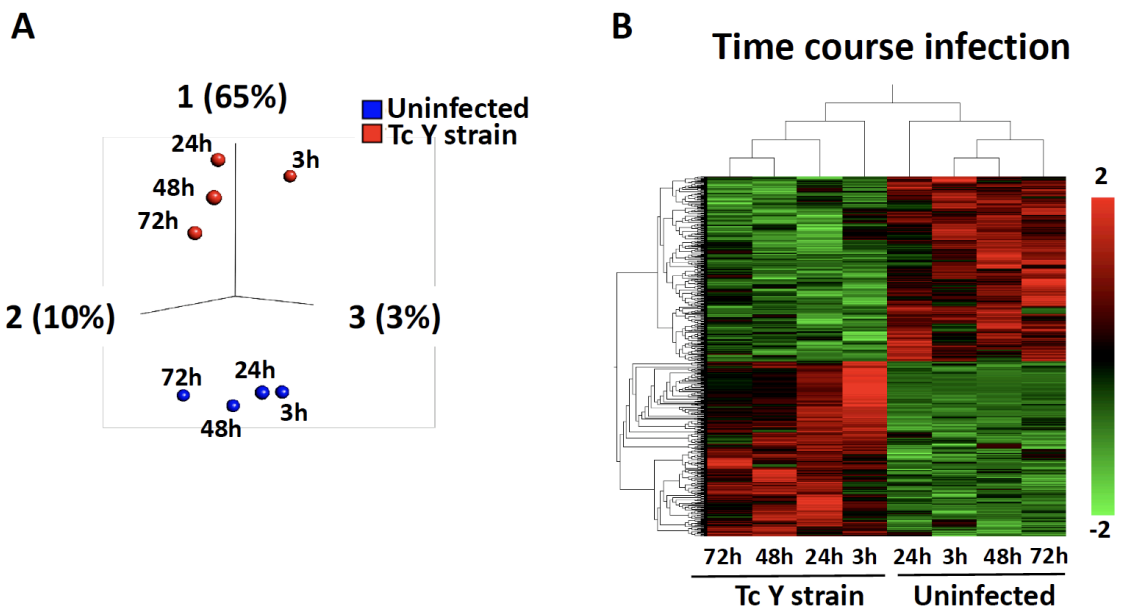

Figure S3. Related to Figure 4. RNA-seq of iPSC-CMs Infected with *Trypanosoma cruzi*. Correlations between uninfected and infected (Tc Y strain) iPSC-CMs at different times. **(A)** PCA with computation of closest neighboring samples. **(B)** Heat map shows the hierarchical clustering.

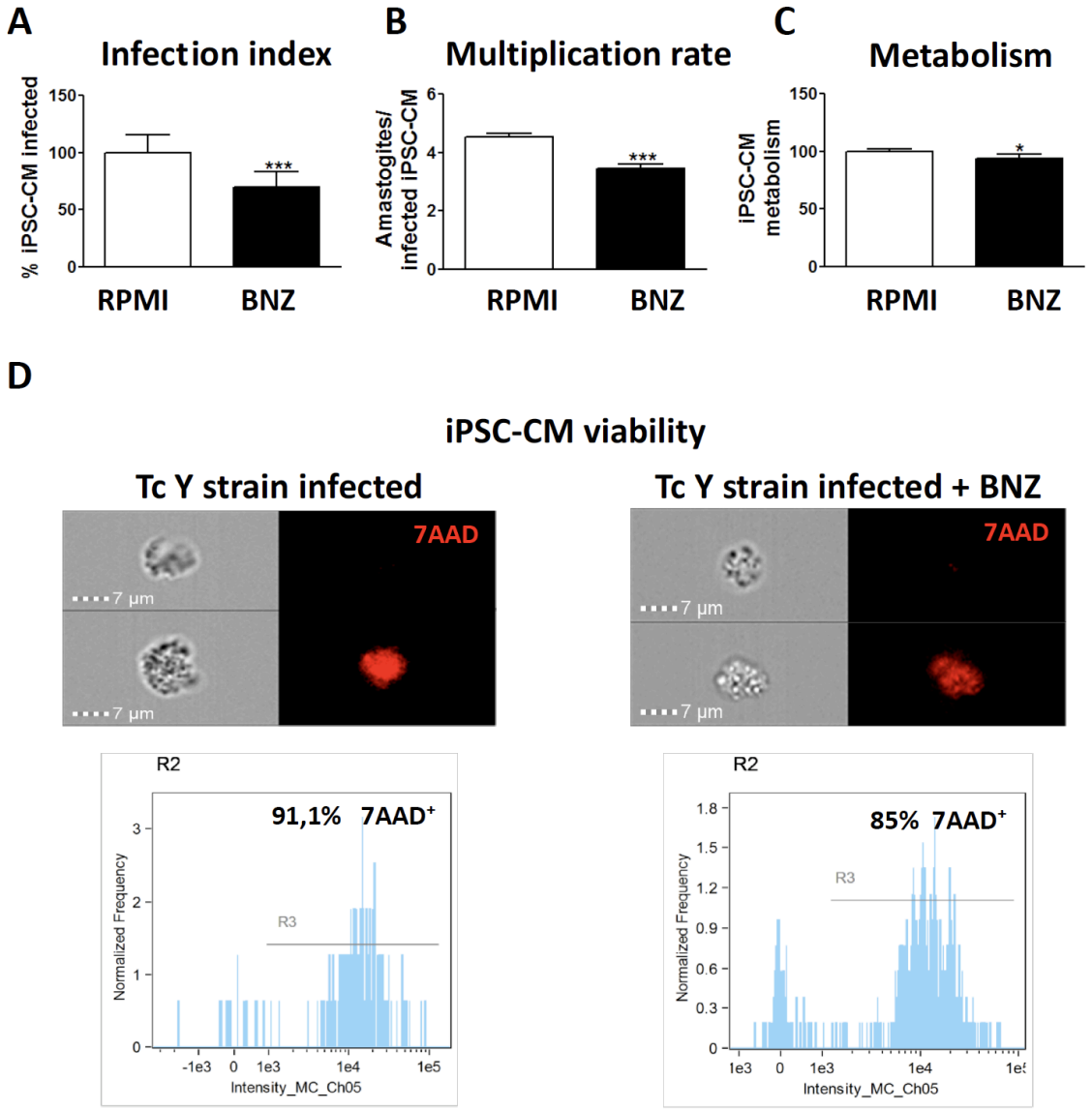

Figure S4. Effects of Benznidazole on *T. cruzi* Infected iPSC-CMs, Related to Discussion of iPSC-CM Model as a Platform to Screening New Drugs to ChD. Human iPSC-CMs infected with Tc Y strain *T. cruzi* show decrease in **(A)** infection index, **(B)** multiplication rate, and **(C)** metabolism when treated with 3.8 µM BNZ. The average of biological triplicates is expressed in graphs. Significant statistical ($p<0.05$) differences are indicated between samples. *$p<0.05$, ***$p<0.001$. **(D)** FACS analysis shows improvement in cell viability of iPSC-CMs infected with Tc Y strain *T. cruzi* when treated with 3.8 µM BNZ.

Supplemental Experimental Procedures

Generation of iPSCs. Reprogramming with the Sendai virus was used to generate three human iPSC lines from peripheral blood mononuclear cells (PBMCs) of three healthy individuals. iPSC colonies were maintained in an Essential 8 medium (E8) (Life Technologies, CA, USA) and dissociated with 0.5 mM EDTA into a single-cell suspension using E8 medium containing 10 μM ROCK inhibitor (Sigma, MO, USA).

Parasites. Culture-derived trypomastigotes (TCTs) of the Y strain were obtained from monolayers of Vero cells (ATCC® CCL-81TM, VA, USA), which were infected at a ratio of 5:1 (TCTs:Vero cells). Vero cells were incubated at 37°C in RPMI medium enriched with 5% inactivated FBS supplemented with antibiotics. Parasites were collected from the culture supernatants by centrifugation at 1000 x g for 10 min and the sediment was suspended in RPMI medium plus 5% FBS. Parasites thus obtained were counted in a Neubauer chamber and the number adjusted according to each assay.

Immunofluorescence. For indirect immunofluorescence, iPSC-CMs (1.5×10^5) grown on Matrigel (BD Biosciences, Franklin Lakes, New Jersey, USA)-coated coverslips of an 8-well chamber slide were fixed with 4% paraformaldehyde in phosphate-buffered saline (PBS) (pH 7.2) for 15 min at room temperature (RT) and permeabilized with 0.1% Triton X-100 (Sigma, Chemical Company, St. Louis, MO, USA) for 15 min at RT. The cells were incubated overnight at 4ºC with rabbit anti-human alpha actin (Sigma, catalog # SAB5600071), mouse anti-human troponin T (Invitrogen, catalog # MA1-26935, Waltham, Massachusetts, USA), rabbit anti-human troponin T (Abcam, catalog # ab45932, Cambridge, United Kingdom), rabbit anti-human BDKRB1 (Abcam, catalog # ab75148), rabbit anti-human BDKRB2 (Abcam, catalog # ab236093), rabbit anti-human cortactin (Abcam, catalog # ab81208), or rabbit anti-human Connexin 43 (Abcam, catalog # ab217676, Cambridge, United Kingdom), diluted in 2% goat serum (GS) in PBS. After washing four times with 1% GS, the cells were incubated for 1 hr at room temperature with the secondary antibody, goat anti-mouse immunoglobulin G (IgG) Alexa Fluor 488, or goat anti-rabbit IgG Alexa Fluor 594 (Thermo Fisher Scientific, Waltham, Massachusetts, USA). The cells were washed four times and one drop of mounting medium (Slow Fade Gold Antifade; Thermo Fisher Scientific) with 4',6-diamidino-2-phenylindole (DAPI) was used for imaging, which was performed using a fluorescence hybrid microscope (Echo Laboratories, San Diego, CA, USA).

Giemsa staining. To quantitate the *T. cruzi* infection on iPSC-CMs, Giemsa staining was performed. Approximately 2×10^5 iPSC-CMs/well were seeded into each well of an 8-well chamber slide (Nunc, Waltham, Massachusetts, USA). Cells were allowed to settle for 48 hr before the invasion assay with 10^6 parasites, as described previously. After 24, 48, 72, and 96 hr, the iPSC-CM were stained with Giemsa (Sigma). The cells were fixed with Bouin's fixative solution (Sigma) for 10 min and washed with 0.15M PBS twice. Then cells were incubated overnight with Giemsa solution diluted 1:20 in water and buffered to pH 6.8. Chamber slides were rinsed with water and air-dried. The cells were analyzed using a light microscope (Leica Microsystems, Wetzlar, Germany) at 1000x magnification.

Viability assay. Viability of iPSC-CMs was analyzed using 7-Amino-Actinomycin D (7-AAD) (BD pharmingen, San Diego, California, USA) nucleic acid dye. 1×10^5 iPSC-CMs were seeded in a pre-coated 96-well plate in RPMI/B27 plus insulin medium. Following 24 hr at 37ºC at 5% CO_2, iPSC-CMs were infected with *T. cruzi* Y strain at a 1:5 (cells:parasites) ratio. After 3 hr interaction time, medium was replaced for another 72 hr. Cells were stained with 5 μL (0.25 μg) of 7-AAD for 10 min at 20ºC and washed with PBS. 7-AAD fluorescence was detected in the far-red range of the spectrum (650 nm long-pass filter) in the ImageStream®X Mark II Imaging Flow Cytometer (Burlington, Massachusetts, USA). The viability was estimated by taking the percentage of cells not stained with 7-AAD once this dye is efficiently excluded by intact cells.

iPSC-CM counting. DAPI reagent (Invitrogen) was used to determine the number of iPSC-CMs cultured with *T. cruzi*. The invasion assay was performed in 24-well plates with 2×10^5 iPSC-CM and 10^6 parasites per well, as described above. The number of iPSC-CMs was accessed at 24, 48, 72, and 96 hr after invasion. The cells were fixed with 4% paraformaldehyde in PBS (pH 7.2) for 15 min at room temperature and stained with DAPI. Using a fluorescence plate reader (Cytation 5 multi-mode reader - BioTek, Winooski, Vermont, USA), the iPSC-CMs' nuclei were measured, and the *Trypanosoma* nuclei were excluded by size.

Reactive oxygen and nitrogen species assay. To analyze oxidative stress following *T. cruzi* infection, ROS and reactive nitrogen species RNS were measured in cell culture supernatants of iPSC-CMs, using

the OxiSelect *in vitro* ROS/RNS assay kit (Cell Biolabs, Inc, San Diego, CA, USA) according to the manufacturer's instructions. Using a plate reader (Promega, Madison, Wisconsin, USA), fluorescence was measured at 480 nm excitation / 530 nm emission. The data are shown as the average of duplicate and triplicate measurements.

Contractility analysis; related to iPSC-CM contractility following *T. cruzi* infection result. iPSC-CM contractility was analyzed before and after infection with Y strain TCTs. The invasion assay was performed in a 6-well plate with 2 x 10^6 iPSC-CMs/well plus 10^7 parasites. Movies were recorded at 24, 48, and 72 hr of the infection using an inverted microscope (Leica) and Leica LMD software. iPSC-CM contractility was analyzed online using the Cellogy service (www.pulseservice.cellogy.com).

Cytokine and chemokine analysis. The human 63-plex kit (eBiosciences/Affymetrix, MA, USA) was used according to the manufacturer's recommendations, with modifications as described below. Briefly, beads were added to a 96-well plate and washed in a Biotek ELx405 washer. Filtered supernatant (0.25 μm) of iPSC-CMs cultured with TCTs for 24 or 48 hr was added to plates containing mixed antibody-linked beads and incubated at room temperature (RT) for 1 hr, followed by overnight incubation at 4°C with shaking. Cold and RT incubation steps were performed on an orbital shaker at 500-600 rpm. Following overnight incubation, plates were washed in a Biotek ELx405 washer and the biotinylated detection antibody was added for 75 min at RT with shaking. The plate was washed and streptavidin-PE (Luminex, TX, USA) was added. After incubation for 30 min at RT, a wash was performed and reading buffer was added. Each sample was measured in duplicate. Plates were read using a Luminex 200 instrument with a lower boundary of 50 beads per sample per cytokine. Custom assay control beads by Radix Biosolutions (TX, USA) were then added to all wells.

RNA-sequencing. RNA was isolated from frozen pellets of iPSC-CMs using the Qiagen RNeasy kit (Qiagen, Germany) according to the manufacturer's instructions. Libraries for RNA-seq were prepared from 10 ng RNA using the AmpliSeq Transcriptome Human Gene Expression kit (Life Technologies). Briefly, reverse transcribed RNA (cDNA) was prepared, and targets were amplified with Ion AmpliSeq Transcriptome Human Gene Expression Core Panel. Primer sequences were partially digested, linked to adapters and Ion XpressTM Barcode X, and purified using AMPure XP reagent. The library was quantified by PCR and diluted to 50 pM. Samples were sequenced in the Ion Torrent Platform (Thermo Fischer, MA, USA) according to the manufacturer's instruction.

Drug assay. Drug assay was performed with benznidazole (BNZ) to analyze infection index, multiplication rate of parasite, metabolism, and viability of iPSC-CMs. For infection index and multiplication rate analyzes, monolayer of iPSC-CMs was prepared on 8-well chamber slides at a density of 2 x 10^5 cells/well and further cultivated for 48 hours at 37°C in a 5% CO_2 atmosphere. The iPSC-CMs was cultured in chamber slides pre-coated with Matrigel, and RPMI 1640 plus B27 with insulin. The infection was accessed in a target effector ratio of 1:5 (cell:parasite) at 24 hr in the presence of Benznidazole (BNZ) 3.8μM. Then, cells were washed with PBS 0.15M, fixed with Bouin's fixative solution, and stained with Giemsa, as described previously. Infected cells were defined as at least 1 amastigote/cell. The number of infected cells (infection index) as well as the number of amastigotes per infected cells (multiplication) was determined for each vision field by microscopy. For comparison to BNZ-treated wells, control infections (without BNZ) were regarded as 100%. Cell metabolism of iPSC-CMs uninfected was determined by 2,3-bis(2-methoxy-4-nitro-5-sulfophenyl)-2H-tetrazolium-5-carboxanilide inner salt (XTT) (Sigma-Aldrich, St. Louis, MO) metabolic assay. Into a 96 well plate 10^5 cells were seeded, and allowed to settle for 24 hr at 37ºC at 5% CO_2 and 80% humidity. After medium change, BNZ were added, and cells were incubated for 24 hr at 37ºC at 5% CO_2 and 80% humidity. XTT with menadione (Sigma-Aldrich) (200 μg/ml, 40 μM in a volume of 100 μl) in RPMI with 5% FBS (containing B27 for cardiomyocyte tests) were added to each well and incubated at 37ºC. Tests were evaluated using a plate reader (Opsys MR, DYNEX Technologies, Chantilly, VA).